Carbon 200 (2022) 227–235

Contents lists available at ScienceDirect

Carbon

journal homepage: www.elsevier.com/locate/carbon

Controlling the electrochemical hydrogen generation and storage in graphene oxide by *in-situ* Raman spectroscopy

Adrián Pinilla-Sánchez [a], Emigdio Chávez-Angel [b], Sebastián Murcia-López [c], Nina M. Carretero [c], Sidney M. Palardonio [a], Peng Xiao [b,d], Daniel Rueda-García [b], Clivia M. Sotomayor Torres [b,e], Pedro Gómez-Romero [b], Jordi Martorell [a,f], Carles Ros [a,*]

[a] *ICFO - Institut de Ciències Fotòniques, The Barcelona Institute of Science and Technology, 08860, Castelldefels, Spain*
[b] *ICN2 - Catalan Institute of Nanoscience and Nanotechnology, CSIC and The Barcelona Institute of Science and Technology (BIST), Campus UAB, Bellaterra, 08193, Barcelona, Spain*
[c] *IREC - Catalonia Institute for Energy Research, Jardins de les Dones de Negre 1, 08930, Sant Adrià de Besòs, Spain*
[d] *Departament de Física, Universitat Autònoma de Barcelona, Bellaterra, 08193, Barcelona, Spain*
[e] *ICREA, Passeig Lluis Companys 23, 08010, Barcelona, Spain*
[f] *Departament de Física, Universitat Politècnica de Catalunya, 08222, Terrassa, Spain*

ARTICLE INFO

Keywords:
Hydrogen storage
Energy storage
Electrochemical reduction
Hydrogenation
Graphene oxide
Reduced graphene oxide

ABSTRACT

Hydrogen, generated from water splitting, is postulated as one of the most promising alternatives to fossil fuels. In this context, direct hydrogen generation by electrolysis and fixation to graphene oxide in an aqueous suspension could overcome storage and distribution problems of gaseous hydrogen. This study presents time-resolved determination of the electrochemical hydrogenation of GO by *in-situ* Raman spectroscopy, simultaneous to original functional groups elimination.

Hydrogenation is found favoured by dynamic modulation of the electrochemical environment compared to fixed applied potentials, with a 160% increase of C–H bond formation. Epoxide groups suppression and generated hydroxide groups point at these epoxide groups being one of the key sites where hydrogenation was possible. FTIR revealed characteristic symmetric and asymmetric stretching vibrations of C–H bonds in CH_2 and CH_3 groups. This shows that hydrogenation is significantly also occurring in defective sites and edges of the graphene basal plane, rather than H-Csp^3 groups as graphane. We also determined a −0.05 V_{RHE} reduction starting potential in alkaline electrolytes and a 150 mV cathodic delay in acid electrolytes. The identified key parameters role, together with observed diverse C-H_x groups formation, points at future research directions for large-scale hydrogen storage in graphene.

1. Introduction

In a world that demands alternative energy sources and energy vectors to Fossil Fuels, hydrogen generated from electrochemical [1,2] or photoelectrochemical [3] water splitting is postulated as one of the most promising alternatives. Despite the existence of a large global market for hydrogen gas, which is widely used in industry (oil refining, ammonia, methanol and steel production) [4], most of it is still generated from fossil fuels. Along with safety concerns [5], an optimized hydrogen storage and distribution remains a significant challenge. Energy losses from the gas pressurization, storage and distribution still limits a wider application.

Graphene oxide (GO) has emerged as one of the best alternatives to produce graphene-derived materials on large-scale due to the lower cost – synthesized directly by exfoliation and oxidation of graphite – and its hydrophilicity given by the oxygen functional groups (OFG) present in the carbon matrix. These OFG can be removed using different methodologies [6–9] to obtain reduced graphene oxide (rGO), with properties ranging in-between GO and graphene. The main application of graphene oxide is as rGO precursor, but during the last decade its use for energy storage has also been considered. Hydrogenation of GO has already been achieved by different methodologies [10,11], and detrapping of the hydrogen has already been reported [12–16]. Recently, electrochemical water splitting on its surface and direct hydrogen bonding in solid-state

* Corresponding author. Institut de Ciències Fotòniques, Organic Nanostructured Photovoltaics group, Castelldefels, Spain.
E-mail address: carles.ros@icfo.eu (C. Ros).

https://doi.org/10.1016/j.carbon.2022.08.055
Received 17 May 2022; Received in revised form 1 August 2022; Accepted 15 August 2022
Available online 20 August 2022

was demonstrated [17], which would solve some of the major problems of hydrogen gas storage and distribution. Computational simulations have predicted OFG local curvature and irregularities to favour C–H bond formation by inducing a sp2-to-sp3 lattice transition [18].

Graphene presents a theoretical hydrogen storage capacity of up to 7.7 wt% [18,19], and percentages of ~5 wt% have already been reported [16,20,21]. However, such results were obtained in harsh chemical environments or highly energetic plasmas. For this reason, electrochemical hydrogenation is as a promising route. It requires inexpensive equipment, is easily scalable and it can be performed at environmental conditions [22].

Several studies have been carried out in a wide range of conditions, leading to different results and conclusions, depending on hydrogenation occurring [12,13,17,23–26] or not [27–30]. Few works have identified the specific hydrogenation sites, differentiating the basal plane, defective sites, pre-existing OFG sites or edges of the GO [13,31]. Specific studies have reported preferential reduction on epoxide rings [27,30,32], while other reports do not point any specific site. It is accepted that H^+ plays an essential role in the electrochemical reduction [23,25] and two specific reduction mechanisms for the epoxide groups have been proposed [12,13,27]. The first one is the partial reduction generating a hydroxyl group and one radical, which leads through a reversible reaction to the reduction of epoxide to form a C–OH/C–H pair (Eq. 1). The second mechanism corresponds to the complete reduction of the epoxide to restore the sp^2 graphene structure (Eq. 2).

However, knowledge on the conditions that favour the reduction mechanism of different OFG and its hydrogenation is still under debate. In this work, we present a fundamental analysis to determine the influence of different parameters such as: substrate, electrolyte pH, time, potential, and cycling potentials in the electrochemical reduction and hydrogenation mechanisms of GO. *In-situ* live Raman spectroscopy has been used to follow the electrochemical reduction, together with ex-situ Fourier transform infrared (FTIR) spectroscopy and other morphological characterization techniques. Voltammetric cycling and chronoamperometries were used as electrochemical hydrogenation techniques, and were found to have influence on the reduction mechanism and to the amount of C–H bonds formation. Other parameters such as pH-dependant retardment of the OFG reduction and H_2 bubbling in the GO/substrate interface were also studied.

2. Materials and methods

A commercial suspension of 4 mg mL^{-1} GO in water from Graphenea (Graphenea Headquarters, San Sebastián, Spain) was used for the electrode preparation. Potassium phosphate salts (K_2HPO_4 and KH_2PO_4, Sigma Aldrich), sulphuric acid (H_2SO_4, Sigma Aldrich) and potassium hydroxide (KOH, Merk) were used to fabricate the electrolytes. GO aqueous suspensions with concentration 4 mg mL^{-1} were prepared by diluting the commercial mother solution with distilled water. The phosphate buffer solutions (KPi) 0.1 M at pH 2 and pH 12, were prepared by diluting K_2HPO_4 or KH_2PO_4 in ultrapure miliQ® water and adjusting the pH with either H_2SO_4 or KOH.

2.1. Graphene oxide electrodes

GO films on graphite (GO-graph) were prepared by drop-casting 100 μL of 4 mg mL^{-1} GO suspension into 1.2 x 1.2 × 0.0254 cm graphite substrates and allowed to dry first at 60 °C in a convection-drying oven for 90 min and then at room temperature overnight. Graphite foil purchased from Alfa Aesar was used as substrate.

2.2. Electrochemical reduction

All electrochemical experiments were carried out using a home-made 5 mL three-electrode PEEK/PTFE electrochemical cell comprised of working electrode (GO-graph or GO-Cu), a counter electrode (platinum wire) and reference electrode (Ag/AgCl/KCl 1 M $E^\circ = 0.222\ V_{RHE}$). The working electrode set up was obtained by pressing the GO film against an O-ring, sealing a small aperture in the electrochemical cell, defining an electrode area of 0.5 cm^2. Experiments were performed in 0.1 M KPi, at either pH 2 or pH 12, as supporting electrolyte. The electrochemical reduction was made by cyclic voltammetry between +0.34 and −1 V_{RHE} (starting and ending at +0.34 V_{RHE}) at different scan rates and cycles, or by chronoamperometry at different potential values and times using a potentiostat model SP-300 Bio-Logic SAS controlled by the EC-Lab software.

2.3. Characterization techniques

Raman spectra were obtained in a Renishaw inVia spectrometer, equipped with a 532 nm wavelength laser and 50x objective. In order to avoid sample damage or laser induced reduction [33], the laser was attenuated to 0.5% power, 4 s exposition time and 8 acquisitions. Raman spectra were fitted to sums of functions using Peak-o-mat 1.2.9 software, using three pseudo-Voigt functions (for D, G and D′ bands) and two Gaussian function (for D* and D″ bands). FTIR spectra were recorded using a Cary 630 FTIR-ATR. The spectra were obtained after compilation of 128 scans at 4 cm^{-1} resolution. The surface morphology of the films was evaluated by field emission scanning electron microscopy (FEG--SEM, FEI Inspect F-EBL). X-ray diffraction (XRD) patterns of GO films were recorded on a Regaku Alpha 1 diffractometer using Cu-Kα (λ = 1.5406 Å) radiation, in the $5^\circ \leq 2\theta \leq 60^\circ$ range at 0.01°/s.

2.3.1. In-situ Raman spectroscopy

A three-electrode 0.5 mL volume home-made PDMS electrochemical cell was used to perform the Raman *in-situ* measurements. The GO film was used as working electrode, a Pt wire as counter electrode and Ag/AgCl 3.5 M as reference electrode. The Raman spectra were recorded by T64000 Raman spectrometer manufactured by HORIBA Jobin Yvon (Chilly-Mazarin, France). It was used in single grating mode (2400 lines)

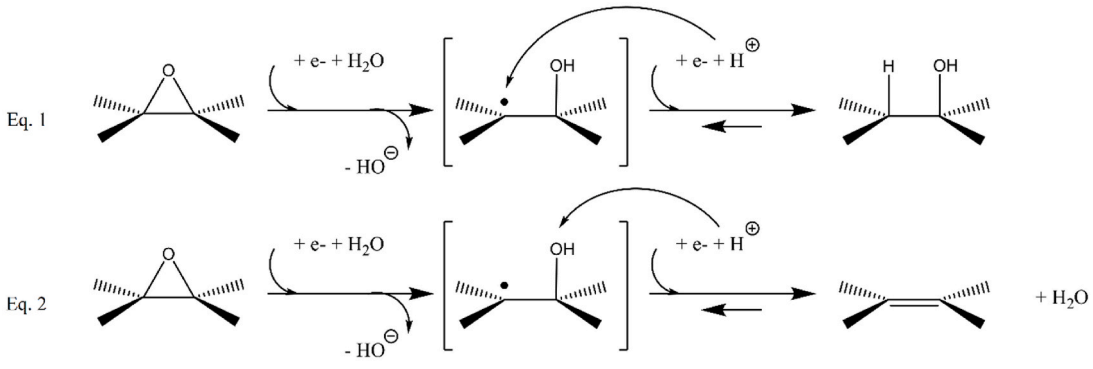

with a spectral resolution better than 0.4 cm^{-1}. The Raman spectra of GO were recorded in the range 1250–1700 cm^{-1} in two different spectral windows. A 532 nm diode laser was focused on the surface of the GO film by using a 10x long working distance microscope objective. Raman spectra were fitted to sums of functions using Peak-o-mat 1.2.9 software, using three pseudo-Voigt functions (for D, G and D′ bands) and fixing D' band position in 1615–1620 cm^{-1}. Error bars were determined from the fitting accuracy.

3. Results and discussion

3.1. GO electrode characterization

Pristine GO electrodes deposited on graphite by drop-casting were characterized by SEM and XRD. SEM (Fig. 1a) shows characteristic graphene nanosheets uniformly distributed and covering the whole substrate. The morphology of the substrate causes the generation of wrinkles and stretch marks. The XRD spectrum (Fig. 1b) shows a (001) diffraction peak at $2\theta = 10.26°$ (d = 8.61 Å). This large interlayer distance is attributed to OFG present in GO, which expand the space between graphitic 2D layers. This is known as a clear sign of the oxidation of graphite into GO [34,35]. In addition, there is a small broad peak at $2\theta = 18.81°$ owing to a disordered component(s) generated during the GO thermal drying process after GO electroreduction [36]. Moreover, it is also observed a (100) diffraction peak at $2\theta = 44.52°$, indicating short range order in stacked GO layers [28].

FTIR-ATR and Raman spectroscopy were used to characterize the starting material and determine the different OFG and oxidation state (Fig. 1c–d). Spectroscopic data shows IR absorption peaks corresponding to vibrations related to different OFG bonded to the carbon lattice. The broad band at 3500-2600 cm^{-1} corresponds to stretching vibrations of –OH bonds, arising from alcohol groups and intercalated water between GO sheets [37]. Two different –OH bending bands appear, corresponding to alcohols (1400 cm^{-1}) and intercalated water (1640 cm^{-1}) [38]. Stretching of C═C from sp^2 domains appears at 1580 cm^{-1}, partially overlapping with intercalated water band. The other main functional group present in the GO, along with alcohols groups, are epoxide rings, showing different C–O stretching bands at 970, 1050 and 1240 cm^{-1} [37]. Meanwhile, the stretching vibrations from C═O corresponding to ketones and carboxylic acids appear at 1730 cm^{-1} and 1800 cm^{-1} respectively [37]. The different OFG can also be classified depending on its location. Mainly, alcohols and epoxides are known to be located in the basal plane while carboxylic acids and ketones in the edges of GO sheets [37].

The Raman spectrum exhibits the typical G (1588 cm^{-1}) band related to vibrations of sp^2 domains and several defect-associated bands (D, D′, D″ and D*), whose position, width and relative intensity depend on the local atomic configuration. Bands D (1354 cm^{-1}) and D' (1615 cm^{-1}) arise when defects (such as OFG attracting C atoms out-of-plane, or defective sites in the C aromatic lattice) break the periodic lattice of graphene, whilst D'' (1540 cm^{-1}) is related to amorphous phases and D* (1150 cm^{-1}) to disordered graphitic lattice due to existence of sp^2-sp^3 bonds [39–43].

The changes in Raman spectra can be interpreted in the framework of the two stage classification introduced by Ferrari [44] for graphene materials. This classification allows us to interpret how variations in defect density influence Raman peaks [44–46]. I_D/I_G ratio was measured to be 1.57 for GO-graph (Table S1), which depending on the average distance between defects (L_D), could correlate to low disorder degree (Stage 1, $L_D > 3$ nm) or to high disorder degree (Stage 2, $L_D < 3$ nm) (Fig. S1). In the case of Stage 2 graphene ($L_D < 3$ nm), the I_D/I_G ratio decreases proportionally to the number of defects instead of increasing, as it would be expected in Stage 1 graphene ($L_D > 3$ nm) [45–47]. For very small L_D, the D band intensity is proportional to the number of 6-fold rings, thus an increase in I_D/I_G indicates ordering and recovery of sp2 domains [44].

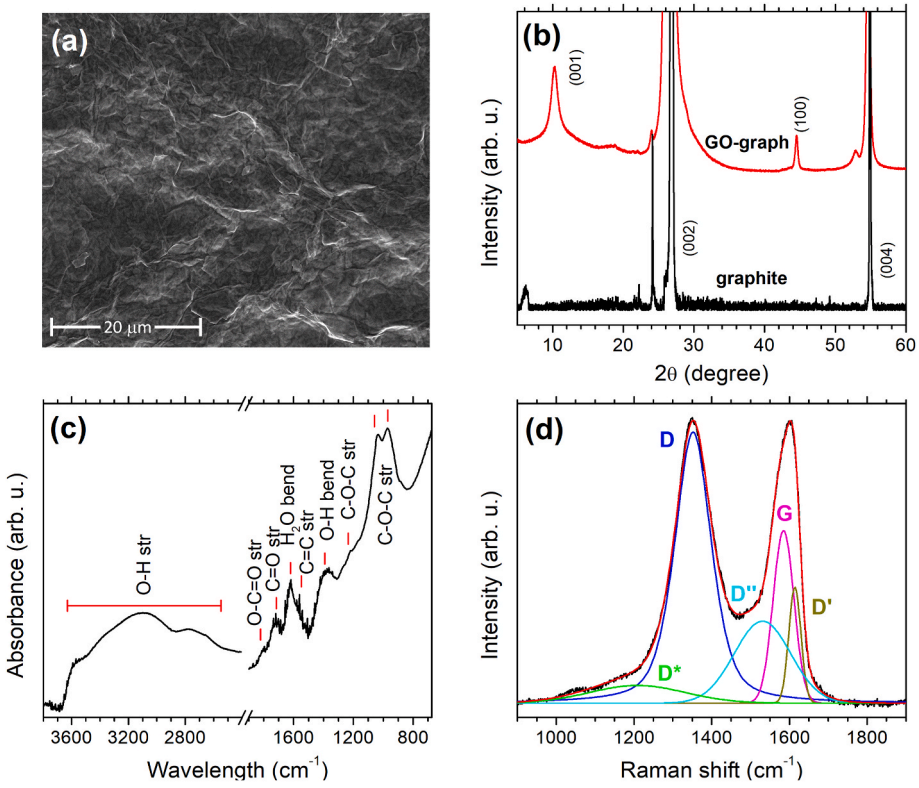

Fig. 1. (a) SEM top view image of a GO-graph sample. (b) XRD diffractogram corresponding to GO-graph (red) and graphite (black), where characteristic peaks of GO can be observed simultaneous to substrate's graphitic peaks. (c) FTIR absorption spectra and (b) deconvoluted Raman spectra of a pristine GO-graph sample. All measurements were performed after electrode fabrication and prior to any modification. (A colour version of this figure can be viewed online.)

To distinguish between Stage 2 and Stage 1 region, the Raman spectra was analysed in terms of full width at half-maximum (FWHM) [45,47]. In our case, the fitted FWHM for D and G bands were 109 and 60 cm^{-1}, respectively, and thus typical of Stage 2 region. Whereas for Stage 1 region FWHM of about 18 and 15 cm^{-1} would be expected, respectively [45,47]. In Stage 2 region, when decreasing the defect density, the Raman spectra evolves as follows: the G and D bands position blueshifts and redshifts, respectively, meanwhile the I_D/I_G ratio increases and FWHM of both D and G band decrease.

3.2. Electrochemical GO reduction at fixed potentials

Initially, GO-graph electrodes were set at open circuit potential (OCP) to track the stabilization potential of the samples in contact with the electrolyte, which were found to be 0.50 and 1.08 V_{RHE} for pH 2 and 12, respectively (Fig. S2). Then, the samples were electrochemically reduced for 60 min in 0.1 M KPi in acid (pH 2) and alkaline electrolytes (pH 12), by applying fixed voltages of −0.45 and −1.25 V vs OCP – corresponding to 0.04 and −0.76 V_{RHE} at pH 2 and 0.63 and −0.17 V_{RHE} at pH 12. To study the reduction mechanisms of the different OFG, the electrodes were characterized ex-situ by FTIR and Raman spectroscopy (Fig. 2).

Both at OCP and at +0.04 V_{RHE} (−0.45 V vs OCP) at pH 2, we did not detect significant changes in the infrared and Raman spectra. But at pH 12, which OCP stabilized at 1.08 V_{RHE} or under applied +0.63 V_{RHE} (−0.45 V vs OCP), a drastic reduction of C═O stretching bands at 1730 and 1800 cm^{-1} was observed. Two new bands appeared at 1575 and 1365 cm^{-1} attributed to carboxylate group ($-COO^-$). The presence of COO^- groups is due to the reaction between alkaline electrolyte hydroxides (-OH) and carboxylic acid groups from GO (-COOH), which loose a proton [26]. The protonation also can explain the changes observed in Raman spectra (Fig. S3, Fig. S4). An enhancement of I_{D^*}/I_G is also observed, commonly associated to the increase of C/O ratio. This enhancement is also associated to an increase of interlayer distance [48]. Moreover, the increase in $I_{D^{**}}/I_G$ ratio also indicates a loss of order [39], being the repulsion between negatively charged carboxylate groups a possible reason for the increase in interlayer distance.

When applying potentials of −0.76 and −0.17 V_{RHE} to GO-graph electrodes (corresponding to −1.25 V vs OCP at pH 2 and 12, respectively), stronger evidence of structural changes was observed. Fig. 2a shows almost complete absence of epoxide rings (1050-850 cm^{-1}), but only a slight reduction in hydroxyl stretching band (3500-2600 cm^{-1}) is observed. Although the C═C stretching band (1580 cm^{-1}) disappears, this does not indicate a reduction of sp^2 domains but rather a recovery of non-OFG-altered hexagonal carbon lattice, which is inactive to IR absorption [25,30]. A slight reduction of intercalated water band is observed.

The Raman spectrum of reduced samples for GO-graph (Fig. 2b) confirms the high reduction degree observed in FTIR. A blueshift and redshift is observed in G and D band (Fig. S4), along with a FWHM sharpening of both bands. That indicates a reduction in the number of defects in high disordered GO [42]. An increase of I_D/I_G (Fig. S3) ratio indicates a restoring of sp^2 domains. Meanwhile, a reduction of $I_{D^{**}}/I_G$ and I_{D^*}/I_G ratio point out a higher order degree and reduction of GO oxygen content, respectively [39,48].

The SEM images (Figs. S5a–b) show an increase in stretch marks along the surface. On the other hand, X-ray diffraction pattern (Fig. S6) displays a splitting of the peak around 10° corresponding to the (001) graphite plane, indicating the existence of two different phases with different interlayer distances of 10.15 Å (2θ = 8.7°) and 7.19 Å (2θ = 12.3°). These two components suggest a differential reduction of the surface and the inner GO film not in contact with water, where protons cannot reach [25].

To understand the impact of substrate on the reduction of GO film, we repeated the experiment using copper substrate (Figs. S7 and S8) following previous work by Ciammaruchi et al. [17]. Spectroscopic data of GO samples reduced on copper (Fig. S8) showed similar reduction degree and OFG removal. However, the FTIR spectra did not show C–H bands, indicating that the main reduction mechanism is the reduction to C═C (Eq. 2). The absence of hydrogenation mechanism in copper substrates may be due to uncontrolled electrical contact problems between the copper substrate and H_2 bubble-detached GO film. The appearance

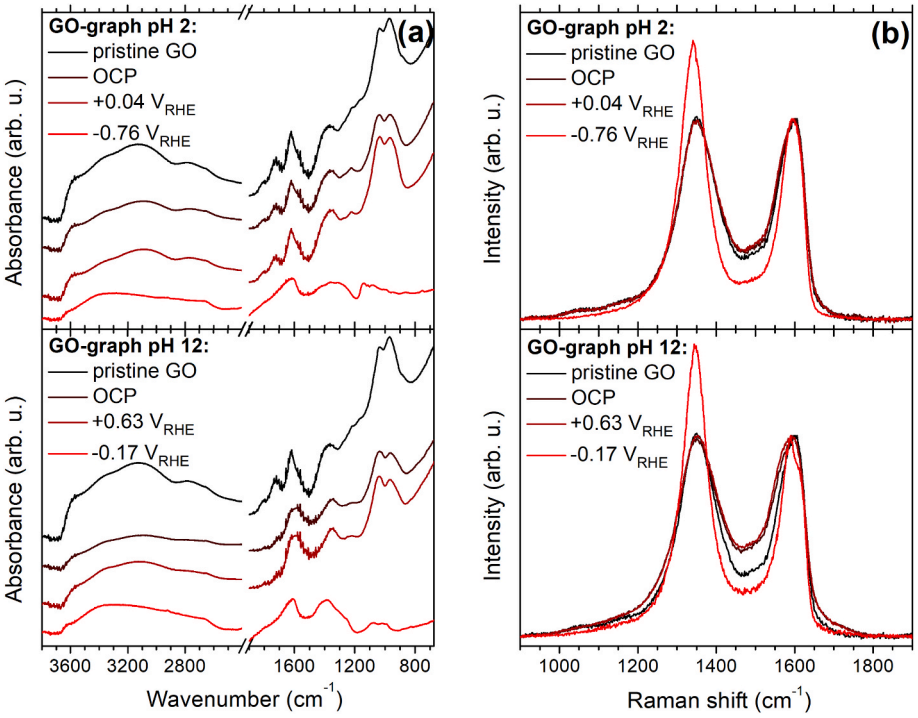

Fig. 2. FTIR absorption spectra (a) and Raman spectra (b) of GO-graph samples as-deposited and after applying different potentials for 60 min, at pH 2 (top) or 12 (bottom). (A colour version of this figure can be viewed online.)

of hydrogen bubbles on the copper surface beneath the GO film caused its total or partial detachment (Fig. S9). The detachment hindered the information related to how long/much time GO was actually polarized.

To further study the role of the pH and potential at which the reduction begins, the process was monitored by *in-situ* Raman spectroscopy. The GO-graph electrodes were electrochemically reduced by applying a 50 mV stepped potential sweep (Fig. 3a and Fig. S10a). Position of D and G bands were followed during the reduction, using a 2400 grid and two different spectral windows for better resolution in frequency.

From stepped potential sweep on GO-graph electrodes, a major blueshift of the D-Band position is observed at −0.2 V_{RHE} for pH 2 and at −0.05 V_{RHE} for pH 12, which can be attributed to the starting reduction potential at each pH. Both starting reduction potentials are located lower than thermodynamic potentials for hydrogen evolution reaction (HER). The variation of the reduction potential with different pH can be caused by the inefficient dissociation of water to initiate the Volmer reaction in alkaline electrolytes, which may favour the reduction of OFG over HER [49,50]. Similar trends have been observed in other works [25].

To further evaluate the influence of the potential and the kinetics of the electrochemical reduction, acidic conditions were selected. This favoured C–H bond formation over OFG reduction [18]. Two different constant voltages of −0.2 and −0.4 V_{RHE} were applied for 30 min in KPi pH 2 (Fig. 3b–d and Fig. S10b). Faster and larger D-Band blueshift, sign of GO electrochemical reduction, was observed for a more negative applied potential. The D and G bands position change mainly happens during the first 5–10 min (Fig. 3b) correlates with the decrease of negative current recorded during the experiment (Fig. 3d).

From the FTIR (Fig. 3c and inset) it can be observed that both GO hydrogenation and loss of OFG in the 1700-800 cm^{-1} range were active at −0.2 V_{RHE}, indicating GO reduction (OFG elimination) takes place simultaneously to HER and C–H bonding. The appearance of C–H stretching bands at 3000-2800 cm^{-1} is observed, along with a small reduction in –OH, C═O and C–O stretching bands. For a more negative potential of −0.4 V_{RHE} there is a slight increase of hydrogenation (C–H stretching band at 2925 cm^{-1}) although a major reduction of the rest of OFG is observed. Therefore, GO hydrogenation level does not become more favoured by increasing potential, but HER becomes more kinetically favoured. This represents less efficient H storage in GO and could end up causing GO film detachment.

To further support the *in-situ* Raman obtained results, different GO-graph electrodes were reduced by applying a constant potential of −0.76 V_{RHE} for 1, 4, 20 and 60 min in 0.1 M KPi pH 2, and characterized ex-situ with FTIR and Raman (Fig. 4). As observed also with *in-situ* Raman spectroscopy (Fig. 3b), hydrogenation and OFG reduction happens during first 4 min (Fig. 4b–c), prior to the negative current peak in the current-time curve (Fig. 4a). Reduced GO shows an increase in I_D/I_G ratio, an upper and lower shift of G and D bands respectively (Fig. 4e–f), indicating high reduction degree and sp^2 recovery. Although, in the minute 4, not all the electrode's area is yet homogeneously reduced (Fig. S11). Some areas show complete reduction while others remain unchanged. By increasing the time to 20 min, the rest of the electrode's surface is reduced completely, and no more changes are observed from 20 to 60 min.

Interestingly, the Raman spectra of GO-graph polarized for 1 min (Fig. 4f) shows a reduction in I_D/I_G ratio, indicating introduction of defects into the structure. This changes may be caused by the introduction of intercalated H^+ (in acid electrolytes) or water molecules in the GO film, observed as deformations of the graphene periodic lattice [51].

3.3. Simultaneous C–H bond formation during electrochemical reduction

Figs. 3c and 4c shown the appearance of four new bands during the reductive process. We observed two strong bands at 2925 and 2850

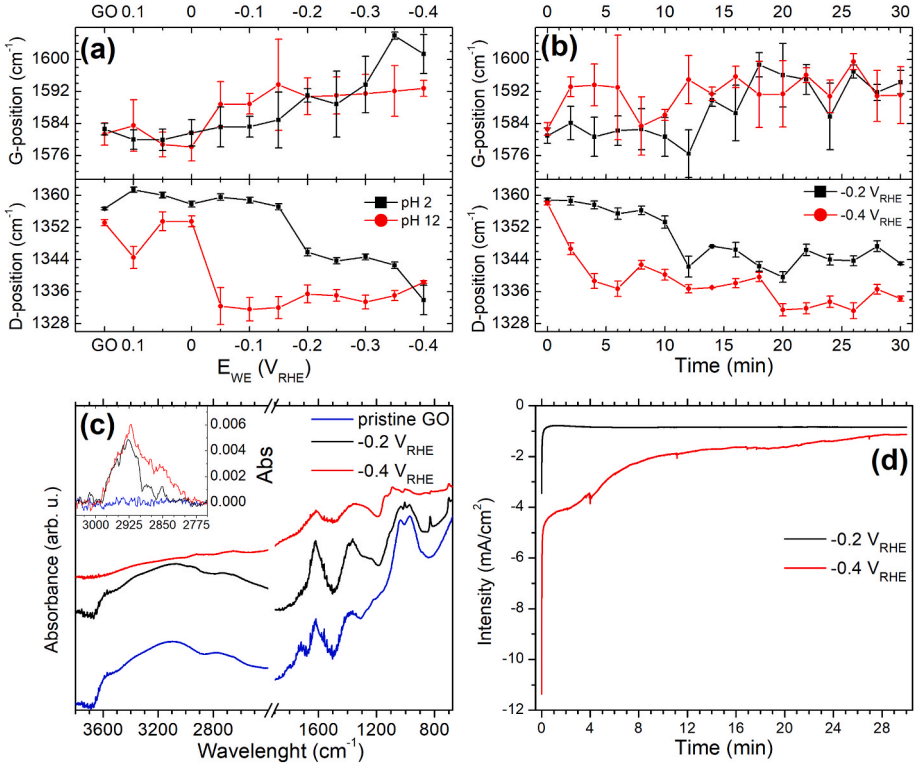

Fig. 3. In-situ measurement of GO-graph G and D Raman shift band positions under (a) an applied stepped potential sweep or (b) a chronoamperometry at different fixed potentials. (c) FTIR and (d) intensity-time curves of samples reduced at different fixed potentials. Measurements were obtained using 0.1 M KPi pH 2 as electrolyte. (A colour version of this figure can be viewed online.)

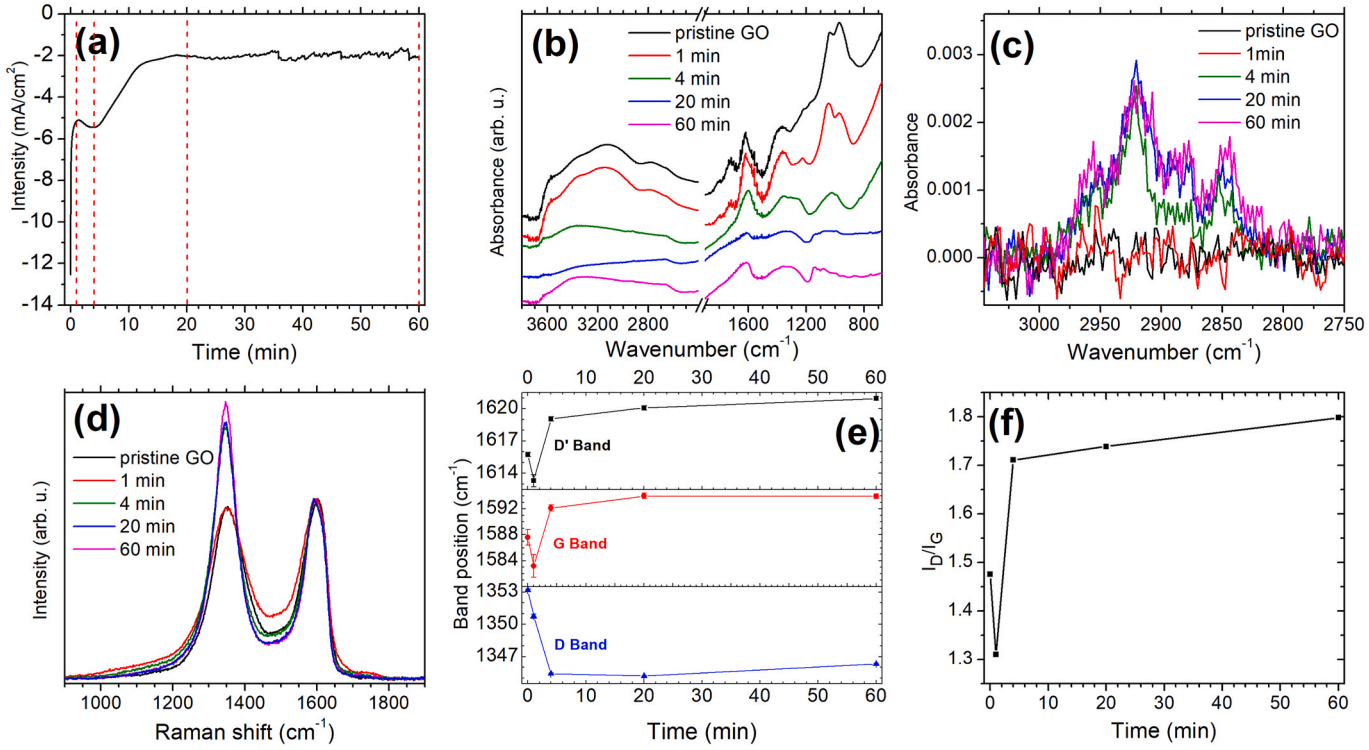

Fig. 4. (a) Intensity-time curve obtained after applying a potential of −0.76 V_{RHE} to GO-graph electrode. (b) FTIR spectra of GO-graph electrodes after applying the same potential for different times. (c) FTIR delimited to C–H stretching region. (d) Raman spectra of the same samples, (e) the position of D, G and D′ bands and. (f) evolution of I_D/I_G ratio. Measurements were obtained using 0.1 M KPi pH 2 as electrolyte. (A colour version of this figure can be viewed online.)

cm^{-1} corresponding to asymmetrical and symmetrical stretching of sp^3 CH_2 groups, and another two at 2950 and 2880 cm^{-1} from asymmetrical and symmetrical stretching of sp^3 CH_3 groups [52]. This indicates hydrogen is being introduced in Csp^3 forming CH_2 and CH_3 moieties.

To better understand the changes observed, it should be taken into consideration the reduction mechanism of epoxides (Eq. 1 and 2). The presence of C–H bands observed in FTIR proves both mechanisms (i.e. C–H and C═C formation) happen simultaneously, being the formation of C–H bands in the ~3000 cm^{-1} region less pronounced than the loss of signal originating from epoxide rings (1050-850 cm^{-1}). This points at epoxide rings reduction into C═C formation (Eq. 2) being favoured over C–H binding (Eq. 1) under the constant-potential applied electrochemical conditions. Furthermore, the low decrease of alcohol associated bands in FTIR, which are expected to be generated along with hydrogenation as following Eq. 1, further support the hydrogenation mechanism of epoxides to be present.

3.4. Electrochemical reduction by cyclic voltammetry

In previous sections, the effect of fixed time and potential was demonstrated. A further comparison of the GO hydrogenation process was performed between chronoamperometry [12,13,17] or cyclic voltammetry [23–26], reported by dew works. GO-graph electrodes were reduced by different number of cyclic voltammetries in the range of +0.34 to −1 V_{RHE} in KPi pH 2. The scan rate was varied from 5 to 20 mV/s and total experiment time was kept at 60 min. The reduction was followed by *in-situ* Raman spectroscopy and analysed ex-situ by FTIR, XRD and SEM.

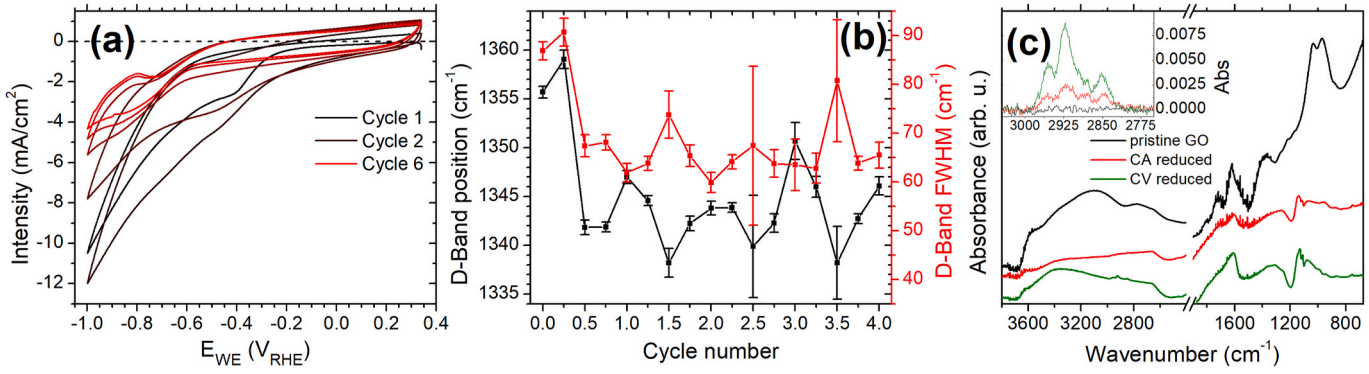

Fig. 5. (a) Cyclic voltammograms of GO-graph electrode at scan rate of 5 mV/s (b) FTIR spectra of GO-graph pristine electrodes (black) and either reduced by chronoamperometry at −0.76 V_{RHE} during 60 min (red) or by cyclic voltammetry between 0.34 and −1 V_{RHE} during 55 min (green). (c) In-situ measurement of D band position and FWHM during cyclic voltammetries. The beginning of each cycle (0.0) corresponds to 0.34 V_{RHE}, one-quarter and three-quarter cycle (0.25 and 0.75) to −0.33 V_{RHE} and half cycle (0.5) to −1 V_{RHE}. Measurements were obtained using 0.1 M KPi pH 2 as electrolyte. (A colour version of this figure can be viewed online.)

Voltammetric curves (Fig. 5a) present both a capacitive behaviour increase (larger difference between the forward and reverse curves in the 0.3 to −0.2 V_{RHE} region) and a shift of the onset potential to negative potentials with successive cycles. A broad reduction peak is observed at −0.4 V_{RHE}, attributed to the reduction of epoxides and carbonyl OFGs [27]. After the second cycle, a change of tendency is observed. The capacitance and the cathodic current in the −0.2 to −1 V_{RHE} region decreases progressively and the reduction peak of OFG almost disappears. It indicates an irreversible reduction of different OFG occur during the first voltametric cycle in the studied range of potentials. With increase of scan cycles a pair of redox peaks appear at −0.9 V, suggesting reversible removal and reformation of some OFGs. This is further proven with the in-situ Raman (Fig. 5b) where it is observed that at positive potentials during cycling there is a recovery of the D and G peaks shift. The cathodic current measured during the first cycles (mainly in the −0.2 to −0.6 V_{RHE} region) perfectly matches the decaying negative current observed in Figs. 4d and 5a when constant potentials of −0.2, −0.4 and −0.76 V_{RHE} are applied. This further confirms the same OFG electrochemical reduction phenomena is happening both when applying cyclic voltammetries or fixed potential chronoamperometries, as observed by *in-situ* Raman spectroscopy in Fig. 4d.

GO-electrodes reduced by cyclic voltammetry can be observed by SEM (Fig. S5c). The images show an increment of wrinkles and porosity, indicating that cyclic voltammetries induce the deformation of the surface and reorganization of the GO flakes. Additionally, the (001) peak in the XRD (Fig. S6) also shows two components, indicating the existence of 2 phases, but with lower interlayer distances: 9.0 Å ($2\theta = 9.8°$) and 7.19 Å ($2\theta = 12.3°$). The porous and wrinkled morphology induced by cyclic voltammetry suggests an increase of water molecules penetration into the film and an increase of the electrochemically active surface and thus, amount of GO active for reduction or hydrogenation. A video has been included as Electronic Supplementary Material to visualize the GO reorganization under electrochemical cycling at negative potentials.

To further study the electrochemical reduction by cyclic voltammetry, the process was followed by *in-situ* Raman spectroscopy measuring at four times at each cycle (at 0.34 → −0.33 → −1 → −0.33 → 0.34 V_{RHE}). If analysing the position and FWHM of D and G bands (D band, Fig. 5b and G band, Fig. S14), the reduction can be divided in two phenomena. During the first scan towards cathodic potential (0.34→-1 V_{RHE}), position and FWHM of D band drop drastically and are not recovered in subsequent cycles, indicating an irreversible reduction. This initial irreversible reduction is consistent with fitted G band position and FWHM trend (Fig. S14). In subsequent cycles, the variations in D positions suggest the GO might be slightly incorporating OFG when scanning towards anodic potential and reduced again when reversing the potential, pointing into a reversible reduction-oxidation process. This initial irreversible step followed by a reversible reaction is in accordance with the first mechanism proposed in Eq. 1 and is consistent with Tateishi [12] and Taniguchi's [13] results.

Comparing the FTIR absorbance spectra of samples reduced by chronoamperometry (CA) or cyclic voltammetry (CV) (Fig. 5c), similar peaks are observed in 800–1700 cm^{-1} region, but also clear differences are displayed in the 2600-3600 cm^{-1} zone. Samples reduced under cyclic voltammetries present more –OH stretching (2600–3600 cm^{-1}) and bending (1400 cm^{-1}) together with increased C–H stretching bands than the ones reduced under −0.76 V_{RHE} constant applied potential. The increase in the C–H bands absorbance was quantified to be a 160% higher than under constant-applied potentials. Additionally, FTIR indicate no dehydrogenation nor OFG formation occur when potential is increased up to 0.34 V_{RHE}. Moreover, 60 min experiments with different scan rates were performed in order to evaluate its influence. It was found the slower the scan rate, the more it favours the hydrogenation mechanism (Figs. S12 and S13). Both C–OH and C–H increased formation under cyclic voltammetries point into a favoured Eq. 1 in front of constant potentials favouring Eq. 2. These results highly support the epoxide groups reduction process being a major one in the hydrogenation process, although other origins for the C–OH and C–H band formation cannot be discarded. The fact that continuous potential cycling result in increased C–H formation can be caused by increased penetration of H^+ ions or water molecules inside the GO film due to variant electrostatic forces, exposing more GO sites to the electrolyte, and to a not ionic depletion of the local electrolyte environment as a constant potential would cause.

Clearly, C–H stretching bands can be separated into characteristic symmetric and asymmetric stretching bands originating from sp^3-bonded CH_2 and CH_3 groups. Thus, this suggests hydrogen is being introduced in out-of-plane Csp^3 in the basal plane or in the edges of GO flakes giving raise to CH_2 and CH_3 moieties. The herein presented electrochemical hydrogenation mechanism of GO results in a hydrogenated reduced GO (rGO:H) differing from graphane (GA) [11], corresponding to a single proton per carbon atom H-Csp^3 moieties – showing a single FTIR absorption peak at 2850 cm^{-1} [53].

4. Conclusions

Graphene oxide, having various oxygen functional groups, was selected as candidate material to study the incorporation of hydrogen. It presented mainly alcohol, epoxides, ketones, and carboxylic acids functional groups, which alter the stable structure of graphene and can help in easing hydrogen electrochemical bonding. Using a simple and scalable electrochemical treatment in water-based electrolytes, hydrogen was incorporated to reduced GO (rGO:H). Simultaneously, OFG were eliminated or reduced, obtaining highly reduced material. The control of these two simultaneous (and in the epoxy site, competitive) reactions was demonstrated possible by using fixed reductive potentials or continuous cyclic voltammetries. This control allowed up to 160% hydrogen storage increase.

Different pH and electrochemical conditions have been studied, aiming at understanding hydrogen incorporation and storage, chemically bonded to GO, and the electrochemical reduction mechanism of GO. Epoxide groups suppression and alcohol groups generated point at epoxide groups sites being one of the sites where hydrogenation was possible. FTIR revealed characteristic symmetric and asymmetric stretching vibrations of C–H bonds in the form of CH_2 and CH_3 groups. This shows that hydrogenation is significantly also happening in defective sites and edges of the graphene basal plane, rather than H-Csp^3 groups as graphane.

In-situ tracking of the main D and G Raman peaks was used to determine the starting potentials of the electrochemical reduction of GO into rGO:H, and −0.2 and −0.05 V_{RHE} were determined for pH2 and pH 12, respectively. The significant difference is attributed to the inefficient dissociation of water to initiate the HER Volmer reaction step in alkaline medium, thus favouring the elimination of OFG. More reductive potentials did not present higher hydrogenation, rather kinetically endorse H_2 gas generation, thus diminishing H storage in GO efficiency.

For constant-applied reductive potential experiments, hydrogen was revealed to be incorporated simultaneous to the observation of a reductive current peak, which also corresponds to the loss of OFG. By further increasing the applied reductive potential, no increase in the hydrogenation was observed, it rather favoured the HER which can end up causing film detachment. On this matter, hydrogen evolution when using a copper substrate quickly leads to GO film detachment, which may be the reason of hydrogenation absence observed.

Cyclic voltammetry has been proven to favour the hydrogenation mechanism over a constant-applied potential, reaching 160% more hydrogen trapping. This is caused by variant electrostatic forces generating a reorganization of the surface that increases electrolyte penetration and thus, the electrochemical active area of GO. The scanning rate is stablished as a governing factor of the reaction, increasing hydrogen trapping when decreasing scanning rate. In situ Raman spectroscopy was used, allowing the identification of two reduction steps: a major

irreversible initial step followed by a minor reversible reaction.

All this shows that precise control of hydrogen incorporation is possible, but faces significant simultaneous functional groups elimination. *In-situ* Raman, correlated with FTIR, is shown as a highly helpful technique to determine starting point of material modification. This work deepens the knowledge in identifying the electrochemical reduction potential of every functional group, in the edges, defects or basal plane of graphene, and in which chemical environment. This work traces the path for additional studies to exploit identified parameters to use this versatile but complex material for large-scale, long term hydrogen storage.

CRediT authorship contribution statement

Adrián Pinilla-Sánchez: Methodology, Validation, Formal analysis, Investigation, Data curation, Writing – original draft. **Emigdio Chávez-Angel:** Methodology, Validation, Investigation, Writing – review & editing. **Sebastián Murcia-López:** Conceptualization, Methodology, Validation, Investigation. **Nina M. Carretero:** Conceptualization, Methodology, Validation, Investigation. **Sidney M. Palardonio:** Validation, Investigation. **Peng Xiao:** Resources, Methodology. **Daniel Rueda-García:** Resources, Methodology. **Clivia M. Sotomayor Torres:** Supervision. **Pedro Gómez-Romero:** Supervision. **Jordi Martorell:** Conceptualization, Writing – review & editing, Supervision. **Carles Ros:** Conceptualization, Methodology, Validation, Formal analysis, Investigation, Writing – original draft, Writing – review & editing, Supervision.

Declaration of competing interest

The authors declare the following financial interests/personal relationships which may be considered as potential competing interests:

Acknowledgements

ICFO and IREC acknowledge financial support from LESGO project (Code: 952068. H2020-EU.1.2.2. funded), BIST Master Program and Severo Ochoa Program. This work was partially funded by CEX2019-000910-S (MCIN/AEI/10.13039/501100011033), Fundació Cellex, Fundació Mir-Puig, and Generalitat de Catalunya through CERCA. ICN2 acknowledge support from Severo Ochoa program, the Spanish Research Agency (AEI, grant no. SEV-2017-0706) and the CERCA Programme/Generalitat de Catalunya. E.C.-A., P.X. and C.M.S.T acknowledge support from Spanish MICINN project SIP (PGC2018-101743-B-I00). P.X. acknowledges support by Ph.D. fellowship from the EU Marie Sklodowska-Curie COFUND PREBIST (Grant Agreement 754558). C.R. acknowledges support from the MCIN/AEI (FJC2020-043223-I) and the Severo Ochoa Excellence Post-doctoral Fellowship (CEX2019-000910-S).

Appendix A. Supplementary data

Supplementary data to this article can be found online at https://doi.org/10.1016/j.carbon.2022.08.055.

References

[1] K. Shinagawa, Tatsuya, Takanabe, Towards versatile and sustainable hydrogen production through electrocatalytical water splitting: electrolyte engineering, ChemSusChem 10 (2017) 1318.
[2] H. Dotan, A. Landman, S.W. Sheehan, K.D. Malviya, N. Hadari, C. Cohen, A. Rothschild, G.S. Grader, Decoupled hydrogen and oxygen evolution by a two-step electrochemical – chemical cycle for efficient overall water splitting, Nat. Energy 4 (2019) 786–795.
[3] Carles Ros, Teresa Andreu, J.R. Morante, Photoelectrochemical water splitting: a road from stable metal oxides to protected thin film solar cells, J. Mater. Chem. A. 8 (2020) 10625–10669, https://doi.org/10.1039/D0TA02755C.
[4] IEA, The future of hydrogen. https://www.iea.org/reports/the-future-of-hydrogen, 2019.
[5] R. Moradi, K.M. Groth, Hydrogen storage and delivery : review of the state of the art technologies and risk and reliability analysis, Int. J. Hydrogen Energy 44 (2019) 12254–12269, https://doi.org/10.1016/j.ijhydene.2019.03.041.
[6] J.F. Rocha, L. Hostert, M.L.M. Bejarano, R.M. Cardoso, M.D. Santos, C. M. Maroneze, M.R. Gongora-Rubio, C. de C.C. Silva, Graphene oxide fibers by microfluidics assembly: a strategy for structural and dimensional control, Nanoscale 13 (2021) 6752–6758, https://doi.org/10.1039/d0nr08380a.
[7] H.L. Guo, X.F. Wang, Q.Y. Qian, F. Bin Wang, X.H. Xia, A green approach to the synthesis of graphene nanosheets, ACS Nano 3 (2009) 2653–2659, https://doi.org/10.1021/nn900227d.
[8] S.Y. Toh, K.S. Loh, S.K. Kamarudin, W.R.W. Daud, Graphene production via electrochemical reduction of graphene oxide: synthesis and characterisation, Chem. Eng. J. 251 (2014) 422–434, https://doi.org/10.1016/j.cej.2014.04.004.
[9] H. Li, C. Bubeck, Photoreduction processes of graphene oxide and related applications, Macromol. Res. 21 (2013) 290–297, https://doi.org/10.1007/s13233-013-1139-x.
[10] K.E. Whitener, Review Article: hydrogenated graphene: a user's guide, J. Vac. Sci. Technol. A 36 (2018), 05G401, https://doi.org/10.1116/1.5034433.
[11] M. Pumera, C.H. An Wong, Graphane and hydrogenated graphene, Chem. Soc. Rev. 42 (2013) 5987–5995, https://doi.org/10.1039/c3cs60132c.
[12] H. Tateishi, M. Koinuma, S. Miyamoto, Y. Kamei, K. Hatakeyama, C. Ogata, T. Taniguchi, A. Funatsu, Y. Matsumoto, Effect of the electrochemical oxidation/reduction cycle on the electrochemical capacitance of graphite oxide, Carbon N. Y. 76 (2014) 40–45, https://doi.org/10.1016/j.carbon.2014.04.034.
[13] T. Taniguchi, K.C. Wong, L. Nurdiwijayanto, K. Hatakeyama, K. Awaya, S. Ida, M. Koinuma, S. Ueda, M. Osada, H. Yokoi, Reversible hydrogenation and irreversible epoxidation induced by graphene oxide electrolysis, Carbon N. Y. 177 (2021) 26–34, https://doi.org/10.1016/j.carbon.2021.02.057.
[14] K.S. Elias, D. C, R.R. Nair, T.M.G. Mohiuddin, S.V. Morozov, P. Blake, M.P. Halsall, A.C. Ferrari, D.W. Boukhvalov, M.I. Katsnelson, A.K. Geim, Novoselov, Control of graphene's properties by reversible hydrogenation: evidence for graphane, Science 323 (80) (2009) 610–613.
[15] L. Gao, P.P. Pal, T. Seideman, N.P. Guisinger, J.R. Guest, Current-driven hydrogen desorption from graphene: experiment and theory, J. Phys. Chem. Lett. 7 (2016) 486–494, https://doi.org/10.1021/acs.jpclett.5b02471.
[16] K.S. Subrahmanyam, P. Kumar, U. Maitra, A. Govindaraj, K.P.S.S. Hembram, U. V. Waghmare, C.N.R. Rao, Chemical storage of hydrogen in few-layer graphene, Proc. Natl. Acad. Sci. USA 108 (2011) 2674–2677, https://doi.org/10.1073/pnas.1019542108.
[17] L. Ciammaruchi, L. Bellucci, G.C. Castillo, G.M.D. Sánchez, Q. Liu, V. Tozzini, J. Martorell, Water splitting for hydrogen chemisorption in graphene oxide dynamically evolving to a graphane character lattice, Carbon N. Y. 153 (2019) 234–241, https://doi.org/10.1016/j.carbon.2019.06.087.
[18] V. Tozzini, V. Pellegrini, Prospects for hydrogen storage in graphene, Phys. Chem. Chem. Phys. 15 (2013) 80–89, https://doi.org/10.1039/c2cp42538f.
[19] M. Pumera, Graphene-based nanomaterials for energy storage, Energy Environ. Sci. 4 (2011) 668–674, https://doi.org/10.1039/C0EE00295J.
[20] A.G. Klechikov, G. Mercier, P. Merino, S. Blanco, C. Merino, A.V. Talyzin, Hydrogen storage in bulk graphene-related materials, Microporous Mesoporous Mater. 210 (2015) 46–51, https://doi.org/10.1016/J.MICROMESO.2015.02.017.
[21] J.M. Kim, W.G. Hong, S.M. Lee, S.J. Chang, Y. Jun, B.H. Kim, H.J. Kim, Energy storage of thermally reduced graphene oxide, Int. J. Hydrogen Energy 39 (2014) 3799–3804, https://doi.org/10.1016/J.IJHYDENE.2013.12.144.
[22] S.A. Iberdrola, Iberdrola builds the largest green hydrogen plant for industrial use in Europe, (n.d.). https://www.iberdrola.com/about-us/lines-business/flagship-projects/puertollano-green-hydrogen-plant.
[23] J.A. Quezada-Renteria, L.F. Chazaro-Ruiz, J.R. Rangel-Mendez, Poorly conductive electrochemically reduced graphene oxide films modified with alkyne chains to avoid the corrosion-promoting effect of graphene-based materials on carbon steel, Carbon N. Y. 167 (2020) 512–522, https://doi.org/10.1016/j.carbon.2020.05.069.
[24] J.A. Quezada Renteria, C. Ruiz-Garcia, T. Sauvage, L.F. Chazaro-Ruiz, J.R. Rangel-Mendez, C.O. Ania, Photochemical and electrochemical reduction of graphene oxide thin films: tuning the nature of surface defects, Phys. Chem. Chem. Phys. 22 (2020) 20732–20743, https://doi.org/10.1039/d0cp02053b.
[25] J.A. Quezada-Renteria, C.O. Ania, L.F. Chazaro-Ruiz, J.R. Rangel-Mendez, Influence of protons on reduction degree and defect formation in electrochemically reduced graphene oxide, Carbon N. Y. 149 (2019) 722–732, https://doi.org/10.1016/j.carbon.2019.04.109.
[26] W.J. Basirun, M. Sookhakian, S. Baradaran, M.R. Mahmoudian, M. Ebadi, Solid-phase electrochemical reduction of graphene oxide films in alkaline solution, Nanoscale Res. Lett. 8 (2013) 1–9, https://doi.org/10.1186/1556-276X-8-397.
[27] A.G. Marrani, A. Motta, R. Schrebler, R. Zanoni, E.A. Dalchiele, Insights from experiment and theory into the electrochemical reduction mechanism of graphene oxide, Electrochim. Acta 304 (2019) 231–238, https://doi.org/10.1016/j.electacta.2019.02.108.
[28] L. Stobinski, B. Lesiak, A. Malolepszy, M. Mazurkiewicz, B. Mierzwa, J. Zemek, P. Jiricek, I. Bieloshapka, Graphene oxide and reduced graphene oxide studied by the XRD, TEM and electron spectroscopy methods, J. Electron. Spectrosc. Relat. Phenom. 195 (2014) 145–154, https://doi.org/10.1016/j.elspec.2014.07.003.
[29] M. Gao, Y. Xu, X. Wang, Y. Sang, S. Wang, Analysis of electrochemical reduction process of graphene oxide and its electrochemical behavior, Electroanalysis 28 (2016) 1377–1382, https://doi.org/10.1002/elan.201501063.
[30] J. Kauppila, P. Kunnas, P. Damlin, A. Viinikanoja, C. Kvarnström, Electrochemical reduction of graphene oxide films in aqueous and organic solutions, Electrochim. Acta 89 (2013) 84–89, https://doi.org/10.1016/j.electacta.2012.10.153.

[31] Z. Yang, Y. Sun, L.B. Alemany, T.N. Narayanan, W.E. Billups, Birch reduction of graphite. Edge and interior functionalization by hydrogen, J. Am. Chem. Soc. 134 (2012) 18689–18694, https://doi.org/10.1021/ja3073116.
[32] A. Viinikanoja, J. Kauppila, P. Damlin, M. Suominen, C. Kvarnström, In situ FTIR and Raman spectroelectrochemical characterization of graphene oxide upon electrochemical reduction in organic solvents, Phys. Chem. Chem. Phys. 17 (2015) 12115–12123, https://doi.org/10.1039/C5CP00942A.
[33] J.S. Mehta, A.C. Faucett, A. Sharma, J.M. Mativetsky, How reliable are Raman spectroscopy measurements of graphene oxide? J. Phys. Chem. C 121 (2017) 16584–16591, https://doi.org/10.1021/acs.jpcc.7b04517.
[34] K. Krishnamoorthy, M. Veerapandian, K. Yun, S.J. Kim, The chemical and structural analysis of graphene oxide with different degrees of oxidation, Carbon N. Y. 53 (2013) 38–49, https://doi.org/10.1016/j.carbon.2012.10.013.
[35] N.M.S. Hidayah, W.W. Liu, C.W. Lai, N.Z. Noriman, C.S. Khe, U. Hashim, H.C. Lee, Comparison on graphite, graphene oxide and reduced graphene oxide: synthesis and characterization, in: AIP Conf. Proc., AIP Publishing LLC, 2017, 150002, https://doi.org/10.1063/1.5005764.
[36] L. Torrisi, M. Cutroneo, V. Havranek, L. Silipigni, B. Fazio, M. Fazio, G. Di Marco, A. Stassi, A. Torrisi, Self-supporting graphene oxide films preparation and characterization methods, Vacuum 160 (2019) 1–11, https://doi.org/10.1016/j.vacuum.2018.11.001.
[37] R.K. Singh, R. Kumar, D.P. Singh, Graphene oxide: strategies for synthesis, reduction and frontier applications, RSC Adv. 6 (2016) 64993–65011, https://doi.org/10.1039/c6ra07626b.
[38] T. Seki, K.Y. Chiang, C.C. Yu, X. Yu, M. Okuno, J. Hunger, Y. Nagata, M. Bonn, The bending mode of water: a powerful probe for hydrogen bond structure of aqueous systems, J. Phys. Chem. Lett. 11 (2020) 8459–8469, https://doi.org/10.1021/acs.jpclett.0c01259.
[39] S. Claramunt, A. Varea, D. López-Díaz, M.M. Velázquez, A. Cornet, A. Cirera, The importance of interbands on the interpretation of the Raman spectrum of graphene oxide, J. Phys. Chem. C 119 (2015) 10123–10129, https://doi.org/10.1021/acs.jpcc.5b01590.
[40] D. López-Díaz, J.A. Delgado-Notario, V. Clericò, E. Diez, M.D. Merchán, M. M. Velázquez, Towards understanding the Raman spectrum of graphene oxide: the effect of the chemical composition, Coatings 10 (2020) 524, https://doi.org/10.3390/coatings10060524.
[41] D. López-Díaz, M. López Holgado, J.L. García-Fierro, M.M. Velázquez, Evolution of the Raman spectrum with the chemical composition of graphene oxide, J. Phys. Chem. C 121 (2017) 20489–20497, https://doi.org/10.1021/acs.jpcc.7b06236.
[42] E.H. Martins Ferreira, M.V.O. Moutinho, F. Stavale, M.M. Lucchese, R.B. Capaz, C. A. Achete, A. Jorio, Evolution of the Raman spectra from single-, few-, and many-layer graphene with increasing disorder, Phys. Rev. B Condens. Matter 82 (2010), 125429, https://doi.org/10.1103/PhysRevB.82.125429.
[43] A.C. Ferrari, J.C. Meyer, V. Scardaci, C. Casiraghi, M. Lazzeri, F. Mauri, S. Piscanec, D. Jiang, K.S. Novoselov, S. Roth, A.K. Geim, Raman spectrum of graphene and graphene layers, Phys. Rev. Lett. 97 (2006) 1–4, https://doi.org/10.1103/PhysRevLett.97.187401.
[44] A.C. Ferrari, J. Robertson, Interpretation of Raman spectra of disordered and amorphous carbon, Phys. Rev. B 61 (2000), 14095.
[45] L.G. Cançado, A. Jorio, E.H.M. Ferreira, F. Stavale, C.A. Achete, B. Capaz, M.V. O. Moutinho, A. Lombardo, T. Kulmala, A.C. Ferrari, Quantifying defects in graphene via Raman spectroscopy at different excitation energies, Nano Lett. 11 (2011) 3190–3196.
[46] A. Eckmann, A. Felten, A. Mishchenko, L. Britnell, K.S. Novoselov, C. Casiraghi, Probing the nature of defects in graphene by Raman spectroscopy, Nano Lett. 12 (2012) 3925–3930.
[47] A. Jorio, E.H.M. Ferreira, M.V.O. Moutinho, F. Stavale, C.A. Achete, R.B. Capaz, Measuring disorder in graphene with the G and D bands, Phys. Status Solidi 247 (2010) 2980–2982, https://doi.org/10.1002/pssb.201000247.
[48] A.Y. Lee, K. Yang, N.D. Anh, C. Park, S.M. Lee, T.G. Lee, M.S. Jeong, Raman study of D* band in graphene oxide and its correlation with reduction, Appl. Surf. Sci. 536 (2021), 147990, https://doi.org/10.1016/j.apsusc.2020.147990.
[49] K. Kakaei, M.D. Esrafili, A. Ehsani, Alcohol oxidation and hydrogen evolution. https://doi.org/10.1016/B978-0-12-814523-4.00007-1, 2019.
[50] M. Zeng, Y. Li, Recent advances in heterogeneous electrocatalysts for hydrogen evolution reaction, J. Mater. Chem. A. 3 (2015) 14942–14962, https://doi.org/10.1039/c9ra09714g.
[51] M. Acik, C. Mattevi, C. Gong, G. Lee, K. Cho, M. Chhowalla, Y.J. Chabal, The role of intercalated water in multilayered graphene oxide, ACS Nano 4 (2010) 5861–5868.
[52] R. Krishna, E. Titus, L.C. Costa, J.C. Menezes, M.R.P. Correia, S. Pinto, J. Ventura, J.P. Araújo, J.A.S. Cavaleiro, J.J.A. Gracio, Facile synthesis of hydrogenated reduced graphene oxide via hydrogen spillover mechanism, J. Mater. Chem. 22 (2012) 10457–10459, https://doi.org/10.1039/c2jm30945a.
[53] D. Bouša, J. Luxa, D. Sedmidubský, Š. Huber, O. Jankovský, M. Pumera, Z. Sofer, Nanosized graphane (C1H1.14)n by hydrogenation of carbon nanofibers by Birch reduction method, RSC Adv. 6 (2016) 6475–6485, https://doi.org/10.1039/c5ra22077g.